Model-Based Interpretation of Groundwater Arsenic Mobility during in Situ Reductive Transformation of Ferrihydrite

Stolze, Lucien; Zhang, Di; Guo, Huaming; Rolle, Massimo

Published in:
Environmental Science and Technology

Link to article, DOI:
10.1021/acs.est.9b00527

Publication date:
2019

Document Version
Peer reviewed version

This is a Post Print of the article published online 22nd May 2019 in Environmental Science & Technology. The publishers' version is available at the permanent link:
https://pubs.acs.org/doi/10.1021/acs.est.9b00527

Model-based interpretation of groundwater arsenic mobility during in-situ reductive transformation of ferrihydrite

Lucien Stolze[1], Di Zhang[2], Huaming Guo[2], Massimo Rolle*[1]

[1] Department of Environmental Engineering, Technical University of Denmark, Miljøvej, Building 115, 2800 Kgs. Lyngby, Denmark

[2] School of Water Resources and Environment, China University of Geosciences, Beijing 100083, China

*Corresponding author phone: +45 45252257; email: masro@env.dtu.dk

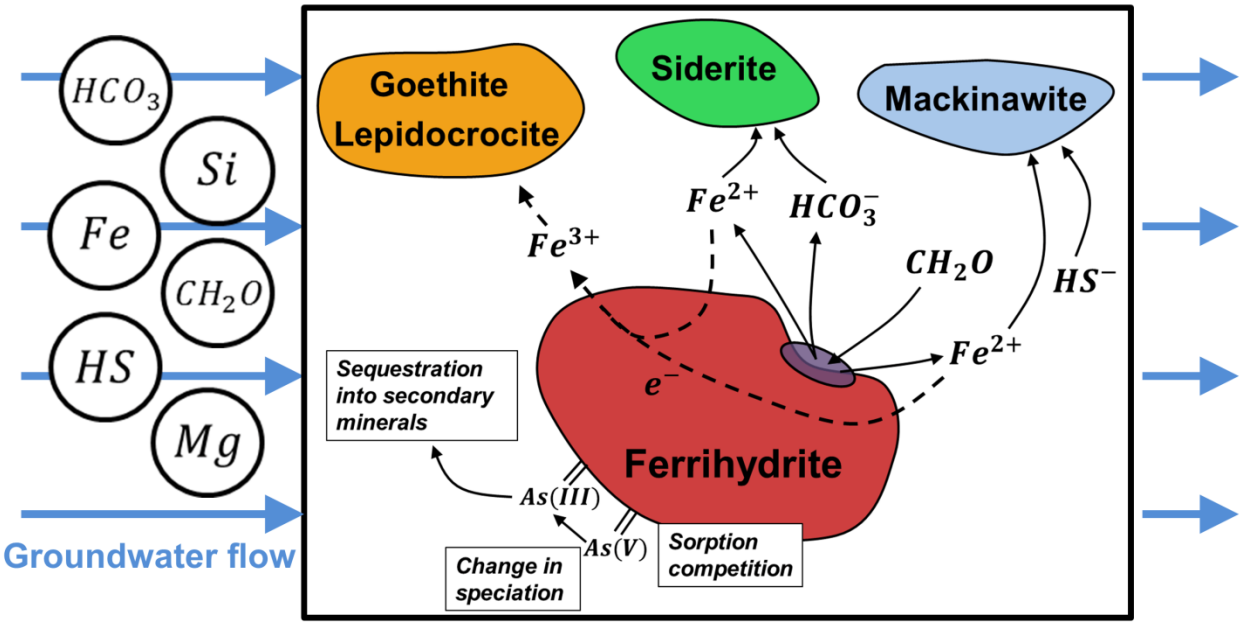

Abstract

Arsenic (As) release and mobility in groundwater is coupled to the iron (Fe) cycling and the associated transformation of Fe-oxides present in sediments. Recent in-situ experiments have provided observations on arsenic mobilization and co-occurring reductive mineral transformation when placing As-loaded ferrihydrite-coated sand for 80 days in wells of an As-contaminated aquifer of Northern China. However, the complex temporal change in solid-associated arsenic and the multiple geochemical processes occurring when the flowing groundwater contacts the As-loaded ferrihydrite-coated sand hamper a detailed evaluation of the experimental dataset. In this study, we develop a modeling approach that allows a quantitative interpretation of arsenic release and ferrihydrite transformation observed during the in-situ experiments. The model accounts for the interplay of abiotic and biotic geochemical processes (i.e., surface complexation, reductive dissolution, formation of secondary iron minerals and arsenic sequestration into the newly formed minerals) involved in the transformation of Fe-oxides and controlling arsenic mobility. The results show the capability of the proposed approach to reproduce the temporal trends of solid arsenic and ferrihydrite concentrations, as well as the spatial variability of mineral transformation, observed in different wells using a common set of surface complexation parameters and kinetic rate constants. The simulation outcomes allowed us to disentangle the specific contribution of the different mechanisms controlling the release of arsenic. It was possible to identify an initial rapid but minor release of As (13-23% of the initial surface concentration) due to desorption from ferrihydrite, as well as the reduction of adsorbed As(V) to As(III) upon contact with the flowing anoxic groundwater. Successively, reductive dissolution of ferrihydrite caused the decrease of the amount of the Fe mineral phase and led to a major depletion of solid-associated arsenic. The produced Fe(II) catalyzed the ferrihydrite conversion

into more crystalline Fe(III) oxides (i.e., lepidocrocite and goethite) through Ostwald ripening, and resulted in the formation of siderite and mackinawite upon reaction with carbonates and sulfides naturally present in the groundwater. The model results also showed that, whereas the decrease in surface sites during reductive dissolution of ferrihydrite promoted arsenic mobilization, the mineral transformation limited As release through its sequestration into the newly formed secondary mineral phases.

Introduction

Prolonged exposure to arsenic (As) contaminated groundwater affects the health of millions of individuals in various parts of the world *(1-3)*. This problem is particularly severe in South East Asia *(4)* where arsenic contamination primarily results from the reducing conditions prevailing in the aquifers, triggering the dissolution of iron oxides present in the sediments and the simultaneous release of As *(5-8)*. The mobility of arsenic in groundwater is controlled by iron minerals through sorption onto the mineral surfaces *(9-13)*. Other important processes, such as the reduction of arsenate to arsenite, can change the affinity for mineral surfaces and affect arsenic mobility *(14-16)*.

Significant effort has been devoted to the investigation of the cycling of iron oxides and its fundamental implications on arsenic release and transport. Ferrihydrite, which has a high capacity in hosting arsenic *(17)*, has been detected in sediments of Bangladesh *(18-19)* and near-surface sediments in the Mekong Delta *(20)* where groundwater arsenic contamination occurred. This poorly crystalline oxide is reactive and can undergo microbially-mediated reductive dissolution *(21-22)*. Furthermore, ferrihydrite can adopt, over time, a more crystalline structure (e.g., goethite), which causes a decrease in the As sequestration potential of the sediments *(13)*. The ferrous iron produced during the reductive dissolution of ferrihydrite can (i) abiotically catalyze the crystallization of the Fe(III) oxide phases *(23-26)* and/or (ii) precipitate into Fe(II)-bearing mineral phases such as siderite, mackinawite, vivianite *(12, 21, 27)*. Depending on the type of secondary mineral phases, significant amount of arsenic can be sequestered through adsorption and reincorporation leading to a disparity between the disintegration of ferrihydrite and the arsenic release *(28-32)*.

The interpretation and prediction of arsenic fate in the subsurface is particularly challenging as it requires the consideration of the complex interplay between flow, reactive transport processes and the hydrochemistry of the groundwater. Despite the large number of studies on arsenic release and transport mechanisms an apparent research gap still exists between the level of understanding of arsenic mobility under controlled laboratory conditions and under natural field conditions. Laboratory studies typically limit the number of geochemical processes under investigation using simplified aqueous composition and mineral assemblage. In contrast, natural systems have a higher level of complexity due to the large number of geochemical factors and co-occurring mechanisms. Hence, pilot-scale experiments, directly conducted in aquifer systems, are of primary importance to bridge such knowledge gap between simplified laboratory setups and complex field investigations. Recently performed pilot-scale experiments, injecting reactive organic compounds to stimulate microbial activity in the subsurface, have provided insights on the transformation of naturally-occurring mineral phases and their interactions with arsenic *(33-34)*. Another experimental approach that has been adopted in pilot scale experiments consists in assessing the change of known mineral phases exposed to natural groundwater conditions *(33, 36-38)*. Furthermore, important insights and quantitative understanding of arsenic release and transport processes are obtained when experimental observations are interpreted with numerical modelling both at laboratory *(39-42)* and at field scales *(34, 43-45)*.

In this study, we develop a model to simulate the reductive transformation of synthetic ferrihydrite and concomitant release of pre-loaded arsenic exposed to natural groundwater conditions during in-situ experiments performed in an As-contaminated sedimentary aquifer of Northern China *(37)*. Such experiments have shown complex dynamics between arsenic release from ferrihydrite-coated sand and ferrihydrite dissolution/transformation at different spatial

locations. Using the implemented modeling framework, we provide a quantitative interpretation of the experimental datasets comprising (i) time series of total Fe and As solid-associated concentrations, (ii) mineral composition at the end of the experiments and (iii) groundwater hydrochemical data. The modeling outcomes highlight the distinct contribution and the interactions of different geochemical processes controlling the mobilization of arsenic at the field site. Such processes include surface complexation reactions, microbially-mediated reductive dissolution, mineral transformation through Ostwald ripening, formation of secondary mineral phases and As sequestration in the newly formed minerals, and determine the complex trends of arsenic and iron observed at the field site.

Materials and Methods

Experiments and datasets description

The in-situ experiments were conducted in monitoring wells screened in a shallow reducing As-contaminated aquifer in the Hetao Basin (Inner Mongolia, China) and consisted in placing As-loaded synthetic iron mineral phases at screen depth (i.e., [18.5 - 26.2] m) for 80 days in order to observe the effect of the continuous groundwater flow on the As retention and iron mineral transformation. The ferrihydrite coated sand was synthetized according to the method of Schwertmann and Cornell *(46)* and the As loading was performed in the laboratory by using a solid-to-solution ratio of 50 g/L and equilibrating the solid phase with a 500 mg/L As(V) solution. The As-loaded coated sand had a porosity of 0.5, a Fe content of 2.71 mg/g coated sand (i.e., 27 g ferrihydrite/L) and an As content of 213 µg/g coated sand.

The coated sand was divided into amounts of 0.5 g before being deployed in the field, where water could flow homogeneously through the highly permeable porous medium. Periodic sampling of the solid phase allowed measuring the temporal change in solid-associated As and total Fe content after total digestion of the sample, using the microwave-assisted method of Link et al. *(47)*. Reductive dissolution of ferrihydrite and release of arsenic occurred incongruently in all wells as shown by the monitored transient decrease in Fe and As. Synchrotron X-Ray diffraction (XRD) indicated that goethite formation occurred in all wells whereas presence of lepidocrocite was less pronounced and differed among the wells. The difference in mineral phase composition was confirmed by the scanning electron microscopy (SEM) exhibiting varying degree of crystallization. In order to characterize the mineral phase composition and the As oxidation at the end of the experiments, Fe and As K-edge X-Ray absorption spectroscopy (XANES) was conducted at the BL14W beamline of the Shanghai Synchrotron Radiation Facility (SSRF) operated in the energy range [-50 ; 150 eV] with a Si(111) monochromator. Fe K-edge XANES indicated significant formation of siderite and mackinawite during the experiments. As K-edge XANES showed that the oxidation state of As adsorbed onto the ferrihydrite surface partially changed from As(V) to As(III). During the in-situ experiments, the chemical composition of the groundwater was measured at 0, 30 and 80 days in each well. In this study, we consider the datasets collected in 3 wells placed along the main groundwater flow direction and separated by a distance of 2.5 km. The datasets include the average groundwater composition for each well, the temporal change in solid-associated As and Fe, as well as the quantification of the secondary mineral phases at the end of the experiments. Details about the monitoring wells and field data are provided in the Supporting Information, whereas an extensive description of the in-situ experiments is given by Zhang et al. *(37)*.

Modeling approach

The model simulates the groundwater flow through the ferrihydrite-coated sand leading to a change from aerobic to anaerobic conditions, the continuous supply of dissolved groundwater species, the mineral transformation, and the As release/sequestration. Figure 1 displays the location of the 3 considered wells, and a visual representation of the conceptual framework for the proposed approach and of the key biogeochemical processes. The model accounts for a series of processes triggered by the dynamic change in the hydrochemistry: the microbially-driven reductive dissolution of ferrihydrite, the formation of secondary Fe(II) and Fe(III) oxides mineral phases, the change in As redox state, as well as the uptake of As through sorption onto iron oxide surfaces and sequestration into secondary mineral phases.

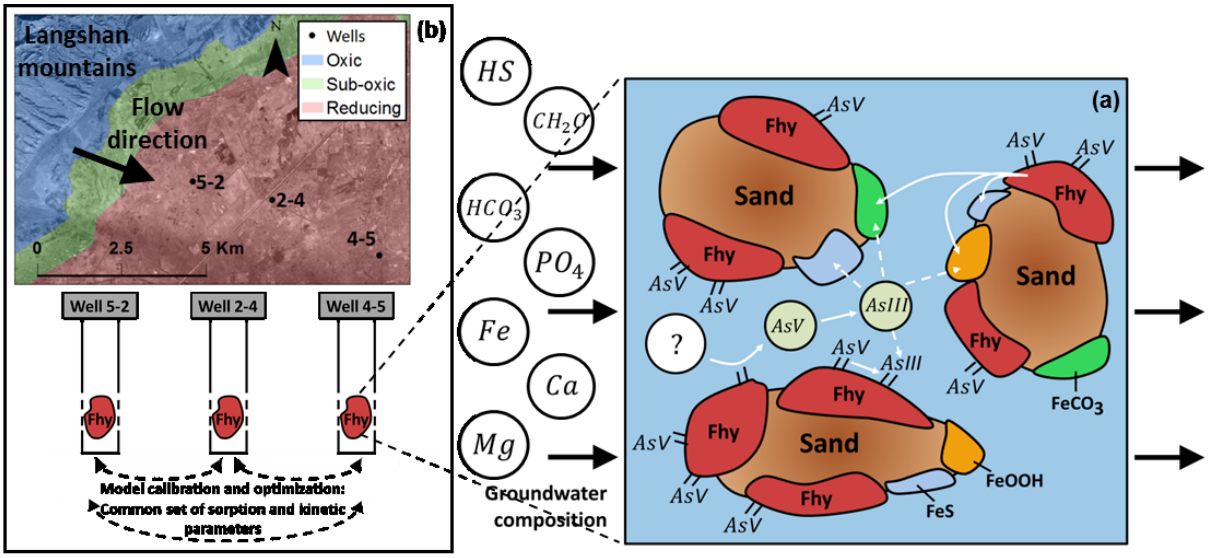

Figure 1. Illustration of the modeling approach for reductive transformation of ferrihydrite and As mobilization/sequestration during the in-situ experiments: (a) conceptual model; (b) location of the observation wells and simultaneous calibration approach through parallelization of simulations with a common set of parameters for the different spatial locations.

133 The first modeling steps consist in loading the arsenic onto the mineral surface by equilibrating
134 ferrihydrite with the As concentrated solution used for the preparation of the reactive samples,
135 and defining the hydrochemical composition of the groundwater according to the field
136 measurements. Subsequently, the solution in contact with the As-loaded ferrihydrite is iteratively
137 replaced by the groundwater solution to simulate the flushing of the pores due to groundwater
138 advection. The flow rates defined through the advective time steps were based on values found in
139 Stolze et al. *(45)* showing decreasing flow velocity along the flow line from the mountains
140 towards the flat plain (Supplementary Information, Table SI7). Following the transport step, the
141 surface complexation reactions and aqueous speciation are calculated assuming local equilibrium,
142 whereas the reductive dissolution of ferrihydrite, the transformation and precipitation of mineral
143 phases, and the change in As speciation were described as kinetic processes. Therefore, the
144 feedback/interaction of the flow and transport processes with the reaction network is directly
145 taken into account in the description of the flow-through system.

146 The model was implemented by coupling the geochemical code PHREEQC-3 *(48)* with the
147 software MATLAB® *(49-50)* using the IPhreeqc model *(51-52)*. Such coupling results in a
148 flexible modeling approach that combines the capabilities of PHREEQC to model solute
149 transport, kinetic and equilibrium reactions with the advanced capability and functions of
150 MATLAB® for data analysis, model calibration and optimization. We used the WATEQ4F
151 thermodynamic aqueous reactions database, amended with the aqueous speciation reactions of
152 arsenic from Dixit and Hering *(17)* (Table 1).

153

Reaction network

The model includes a series of abiotic and microbially-mediated reactions that aimed at describing the geochemical transformations taking place during the in-situ experiments. Table 1 lists the key reactions considered in the model. Ferrihydrite was represented with its simplified stoichiometry $Fe(OH)_3$ for computational ease *(21)*. Secondary Fe(III) phases (i.e., goethite and lepidocrocite) were represented as a generic Fe(III) oxide (FeOOH).

Table 1: Aqueous speciation and geochemical reactions included in the reactive transport model

Aqueous speciation		**log K**
$AsO_4^{3-} + 3H^+ = H_3AsO_4$		20.06[(a)]
$AsO_4^{3-} + 2H^+ = H_2AsO_4^-$		18.35[(a)]
$AsO_4^{3-} + H^+ = HAsO_4^{2-}$		11.60[(a)]
$AsO_3^{3-} + 3H^+ = H_3AsO_3$		34.74[(a)]
$AsO_3^{3-} + 2H^+ = H_2AsO_3^-$		25.52[(a)]
$AsO_3^{3-} + H^+ = HAsO_3^{2-}$		13.41[(a)]
Reactive minerals	**Name**	**log K**
$Fe(OH)_3 + 3H^+ = Fe^{3+} + 3H_2O$	Ferrihydrite	4.891[(b)]
$FeOOH + 3H^+ = Fe^{3+} + 2H_2O$	Fe(III) oxide	-1[(c)]
$FeS + H^+ = Fe^{2+} + HS^-$	Mackinawite	-2.95[(d)]
$FeCO_3 = Fe^{2+} + CO_3^{2-}$	Siderite	-10.89[(c)]
Reductive dissolution of ferrihydrite		
$CH_2O + 4Fe(OH)_3 + 7H^+ \rightarrow HCO_3^- + 4Fe^{2+} + 10H_2O$		
Redox change in As speciation		
$0.5CH_2O + HAsO_4^{2-} + 1.5H^+ \rightarrow H_3AsO_3 + 0.5HCO_3^-$		
$0.5CH_2O + Hfo_wAsO_4^{2-} + 1.5H^+ \rightarrow Hfo_wH_2AsO_3 + 0.5HCO_3^-$		

[(a)]*(17)*, based on MINEQL+ database *(53)*; [(b)] *(54)*, [(c)]*(55)*, [(d)]*(56)*

Dissolution and precipitation kinetics. The mineral transformation reactions were controlled by kinetics rate expressions defined by means of thermodynamic constraints and hydrochemical composition *(57)*. We considered the dissimilatory reductive dissolution of ferrihydrite by oxidation of organic matter leading to the release of Fe(II) and HCO_3^- *(2, 21, 23)*. The kinetic rate of the reaction was expressed as function of the abundance of the electron acceptor (i.e., the

ferrihydrite) with a Monod type rate equation *(41, 57, 58)*. Additional terms allowed us to account for: (i) the decrease in accessibility for reactive surface sites during ferrihydrite dissolution *(59)*, and (ii) the passivation of ferrihydrite via the adsorption of charged species *(60-61)*.

$$R_{ferri} = -k_{ferri}\left(\frac{[Fe(OH)_3]}{K_m^{ferri\text{-}org} + [Fe(OH)_3]}\right)\left(\frac{A_{Fe(OH)_3}}{A_{0,\,Fe(OH)_3}}\right)\left(\frac{S_{tot}-S_{occupied}}{S_{tot}}\right)L(t) \quad \begin{cases} L(t<t_{i,\,ferri})=0 \\ L(t\geq t_{i,\,ferri})=1 \end{cases} \qquad (1)$$

where k_{ferri} is the rate constant, $K_m^{ferri\text{-}org}$ is the half-saturation constant, $A_{Fe(OH)_3}$ and $A_{0,\,Fe(OH)_3}$ are the total surface areas of ferrihydrite at time t and t=0, respectively, S_{tot} is the total amount of ferrihydrite surface sites, and $S_{occupied}$ is the amount of ferrihydrite surface sites occupied by Fe(II) *(60)*, phosphate *(61)*, As(V) *(14, 16)*, silicates, and carbonates. As(III) was not included in the surface site passivation term since it rather favors ferrihydrite dissimilatory reduction *(14)*. Quantities in brackets, [ ], represent the molar concentration of the indicated species. $K_m^{ferri\text{-}org}$ was defined proportional to the amount of Fe(III) crystalline oxide formed during the in-situ experiment, since this can limit ferrihydrite reactivity *(23)*:

$$K_m^{ferri\text{-}org} = K_{m,0}^{ferri\text{-}org}\,\frac{[FeOOH]}{[Fe(OH)_3] + [FeOOH]} \qquad (2)$$

where $K_{m,0}^{ferri\text{-}org}$ is a calibrated variable.

L(t) expresses the inhibition of the reductive dissolution of ferrihydrite for each well over a time period $t_{i,\,ferri,}$ as the dataset indicated a lag phase preceding the decrease in the solid-associated Fe content. The abiotic reduction of ferrihydrite by sulfide was not considered in the model as it was not possible to distinguish its effect from the microbial reductive dissolution of ferrihydrite. The

consumption of organic carbon was simulated according to the reactions and stoichiometry reported in Table 1. Organic carbon was not considered as limiting factor for the reaction kinetics due to its abundance in the flowing groundwater and to its reactivity in the area of the in-situ experiment *(62)*.

The Fe(II)-catalyzed conversion of ferrihydrite into a more crystalline Fe(III) oxide phase (comprising goethite and lepidocrocite) occurs via Ostwald ripening *(16, 24, 63-64)*. The kinetic rate, $R_{Ostwald}$ considers the Fe(II) surface coverage *(21, 30, 65-67)*, the dissolved Fe(II) concentration *(25-26, 68)*, and the effect of chloride, sulfate, and bicarbonate concentrations since these ions have been shown to significantly slow down the crystallization of ferrihydrite *(69)*:

$$R_{Ostwald} = -\left(k_1\left(\frac{S_{Fe(II)}}{S_{tot}}\right) + k_2\frac{[Fe^{2+}]}{[Fe(OH)_3]}\right)\left(\frac{[Fe(OH)_3]}{K_m^{ferri\text{-}ost} + [Fe(OH)_3]}\right)\left(\frac{1}{[Cl^-] + [SO_4^{2-}] + [HCO_3^-]}\right)^x \quad (3)$$

where k_1 and k_2 are rate constants, $S_{Fe(II)}$ is the amount of ferrihydrite surface sites occupied by Fe(II), and x is a calibrated exponent. The abiotic dissolution of ferrihydrite resulting from electron transfer from aqueous Fe(II) is inhibited when the electrochemical potential of the redox couple Fe(II)/Fe(III) exceeds the absolute energy of the conduction band of ferrihydrite (i.e., $E_{Fe(OH)_3} = -5.00$ eV) *(25-26, 68)*. All produced Fe^{3+} was turned into a single Fe(III) crystalline phase. Furthermore, the formation of magnetite was not considered as this mineral was not detected during the in-situ experiments.

Siderite and mackinawite were allowed to precipitate as products of the reaction of Fe(II) from the reactive dissolution of ferrihydrite and dissolved carbonate and sulfide species present in the

flowing groundwater. The precipitation of these secondary minerals was controlled by the kinetic rate expressions:

$$R_{sid\text{-}pptn}=k_{sid\text{-}pptn}\max\left(0,\left[1-\frac{K_{sp(sid)}}{IAP_{sid}}\right]\right) \quad (4)$$

$$R_{mack\text{-}pptn}=k_{mack\text{-}pptn}\max\left(0,\left[1-\frac{K_{sp(mack)}}{IAP_{mack}}\right]\right) \quad (5)$$

where K_{sp} is the solubility product and IAP is the ion activity product.

Arsenic release and sequestration. The change in speciation of arsenic, from As(V) to As(III), occurring when the reduced groundwater contacted the As-loaded ferrihydrite-coated sand, was described as a linear kinetically-controlled mechanisms with a rate coefficient k_{As}. Sorption reactions were assumed to be instantaneous and were modeled for ferrihydrite and the secondary Fe(III) oxide using the diffuse double layer (DDL) model *(70)*. Ferrihydrite was defined with a specific surface area of 600 m^2/g and with weak and strong adsorption sites (i.e., Hfo_w and Hfo_s, respectively) *(70)*. The secondary Fe(III) oxide was assumed to have the surface complexation properties of goethite and was represented with a specific surface area of 54 m^2/g and a single type of surface sites (i.e., Goe) *(71)*. The densities of surface sites Hfo_w and Goe were calibrated within the range [0.05 – 0.31] mol/mol Fe *(17, 72)* and [0.011 - 0.018] mol/mol Fe *(71)*, respectively. The density of Hfo_s sites was set to 0.005 mol/mol Fe *(70)*. Since the number of surface sites are stoichiometrically linked to the mol of mineral phases, reductive transformation of the mineral phases lead to a change in sorption capacity. The set of surface reactions for ferrihydrite was taken from the *(70)* database and amended with arsenic *(17, 73)*, silica *(74)*, carbonates, and ferrous iron *(75)* surface reactions. Ferrihydrite and goethite surface reactions

included in the model with respective equilibrium constants are listed in Tables SI4 and SI5 of the Supplementary Information. The affinity constants for ferrihydrite were re-optimized through calibration using their 95% confidence intervals reported in the literature.

In addition to complexation onto Fe(III) mineral phases, As reincorporation into the crystalline oxides *(32, 76)* and/or adsorption onto siderite *(29)* were considered. These mechanisms were described through the uptake of total aqueous As (i.e., considering the relative proportion of As(III) and As(V)) by a linear sequestration rate stoichiometrically proportional to the amount of produced siderite and secondary Fe(III) oxide defined as:

$$R_{As\text{-}seq}=\alpha\left(R_{sid\text{-}pptn}+R_{Ostwald}\right) \quad (6)$$

where α is the molar ratio of As sequestration. We assumed that no significant amount of As was sequestered by mackinawite *(56, 77-78)*.

Calibration strategy. The modeling framework aimed at describing the reductive mineral transformations and the As release at different spatial locations during the in-situ experiments. We used a common set of parameters between the different spatial locations. Therefore, calibration of the model parameters was performed simultaneously by parallelizing the simulations of the considered observation wells (Figure 1b). The model parameters were calibrated in the MATLAB® environment with an automated procedure minimizing the root mean squared error (RMSE) between simulated and measured solid-associated species (i.e., total As and total Fe) throughout the duration of the experiments. Also the secondary mineral composition representative of the samples at the end of the in-situ experiments and determined by Fe K-edge XANES measurements was included in the calibration. Due to the high number of

parameters and the non-linearity of the problem, the heuristic, global-search particle swarm optimization (PSO) method was chosen to minimize the objective function *(41, 79)*.

Results and discussion

Model-based interpretation of the field observations. The comparison between modeling results and field datasets, displayed in Figure 2, was performed in the three observation wells by considering the temporal change in total solid-associated arsenic (Figures 2a-c), the temporal change in total Fe content (Figures 2d-f), and the amount of iron oxides present in the mineral assemblage at 80 days (Figures 2g-i).

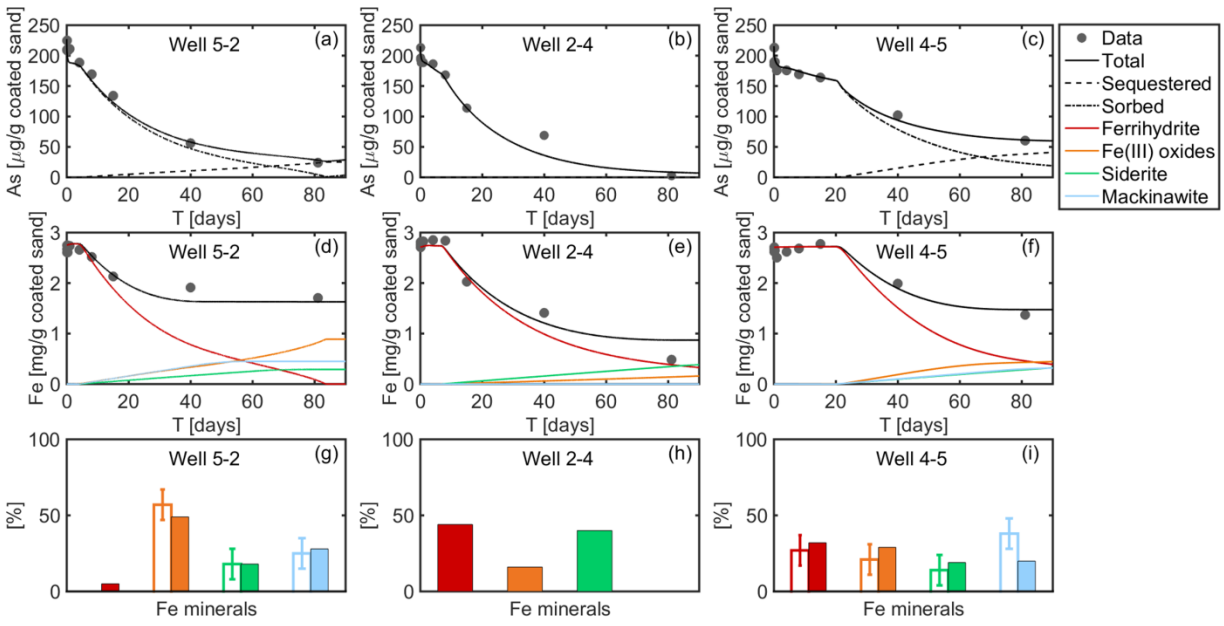

Figure 2. Comparison between experimental data and simulation results. (a)-(c) Dynamic change in total As (note that no sequestered As was predicted in well 2-4); (d)-(f) dynamic change in total Fe and mineral composition; (g)-(i) mineral composition at the end of the experiment: the

253 full and empty bars represent simulated and experimental results determined by XANES,
254 respectively. The error bars show 10% uncertainty on quantified mineral fractions for the
255 XANES data available for wells 5-2 and 4-5.

256 The field data suggest that multiple geochemical processes occurring over different time scales
257 control the As mobilization during the in-situ experiments. Indeed, the solid-associated As
258 concentrations exhibit a complex behavior characterized by a significant and rapid release of
259 arsenic at early time followed by a plateau, particularly visible in wells 2-4 and 4-5, and a
260 subsequent more gradual release. In contrast, decrease in solid-associated Fe did not start when
261 the reactive mineral was exposed to the groundwater but after an initial delay, which was most
262 pronounced in well 4-5. There is a clear consistency between the patterns of As and Fe contents
263 at the different monitoring locations. In particular, the onset of Fe reductive dissolution
264 corresponds to the time at which the arsenic trend shows a change in its slope and starts the
265 gradual decrease which continues throughout the duration of the experiments. The gradual
266 decrease in solid-associated As and the disintegration of the iron mineral phase appears to
267 proceed congruently in wells 2-4 and 4-5. In contrast, in well 5-2 the Fe-content reaches steady
268 state after 40 days whereas the solid-associated As continues to decrease over the whole duration
269 of the in-situ experiments. This difference suggests that the As release cannot be linearly
270 associated with the Fe content. Synchrotron Fe K-edge XANES spectra, available for the
271 samples collected in wells 4-5 and 5-2 at the end of the experiments, show that ferrihydrite was
272 converted into Fe(III) oxide (lepidocrocite, goethite), siderite and mackinawite. In particular,
273 conversion into a more crystalline Fe(III) mineral phase was significantly different in the two
274 wells. Specifically, ferrihydrite was completely consumed and a high amount of Fe(III) oxide

was found in well 5-2, whereas high ferrihydrite and a small amount of Fe(III) oxide were observed in 4-5.

The existence of multiple surface complexation and mineral transformation mechanisms, which significantly differ among the wells, complicates the interpretation of the processes controlling the As release directly from the experimental datasets. The proposed model allowed us to reproduce the field observations in the three wells with a common set of surface complexation parameters and kinetic parameters for mineral transformation (Tables SI4-6). In particular, the sequential release of As from the solid, occurring at different rates, is captured well by the performed simulations. The modeling results show that the sharp decrease in As at early time is due to desorption as no significant transformation of ferrihydrite was taking place. The duration of the lag phase preceding the reductive microbial dissolution of ferrihydrite (i.e., $t_{i,\ ferri}$) was found to vary among the wells (Table SI6). This difference could suggest spatial heterogeneity of this reaction in the field *(20, 80)*. Interestingly, the observed lag phase increases along the selected flow line (i.e. from the mountain towards the flat plain). The model calibrated lag phase appears to scale inversely with the flow velocity and allowed us to reproduce the onset of ferrihydrite disintegration with a similar number (~300) of flushed pore volumes in the three wells. During the reductive dissolution/transformation of ferrihydrite, the solid-associated As concentration becomes function of the As adsorbed onto ferrihydrite and sequestered into the secondary mineral phases. Differences in the calibrated molar ratio of As sequestration α (Table SI6) suggests that this process differs among the wells. In particular, the model predicts that 23, 0, and 38 µg As/g coated sand were sequestered at 80 days in wells 5-2, 2-4, 4-5, respectively even though the amount of crystalline Fe oxides is higher in well 5-2 than 4-5. Furthermore, the model allowed us to reproduce the measured mineral composition for the two wells in which

these measurements were performed. Good agreement was achieved between the observed and simulated amounts of Fe(III) mineral phase, as well as of siderite whereas the model underestimates the amount of mackinawite in well 4-5. The outcomes of the calibrated model are also helpful to visualize the temporal trends of secondary mineral formation and ferrihydrite consumption (Figure 2d-f).

Processes controlling arsenic release. The calibrated model was used to distinguish the contributions of different mechanisms controlling the mobilization of arsenic observed during the in-situ experiments. Here, we assess the effects of arsenic change in speciation, sorption, dissolution of ferrihydrite, and arsenic sequestration into secondary Fe oxides. Figure 3a shows the comparison between simulated solid-associated arsenic for well 4-5 using the calibrated model when individually inhibiting these processes by defining 5 scenarios:

- Scenario A: calibrated model including reduction of adsorbed As(V) to As(III), sorption, reductive dissolution of ferrihydrite, Ostwald ripening, precipitation of ferrous oxides, and arsenic sequestration into the newly formed minerals;
- Scenario B: only sorption processes and reduction of adsorbed As(V) to As(III);
- Scenario C: as Scenario A but without As sequestration into secondary minerals;
- Scenario D: as Scenario A but without the reduction of As(V) to As(III);
- Scenario E: as Scenario A but the change of As(V) to As(III) occurs in the aqueous phase.

Figure 3b displays the simulated temporal change of fractional site occupancy occurring to illustrate the sorption competition mechanism taking place during the in-situ experiments. The

analysis for the other wells has yielded similar results and is reported in the Supporting Information (Figure SI1).

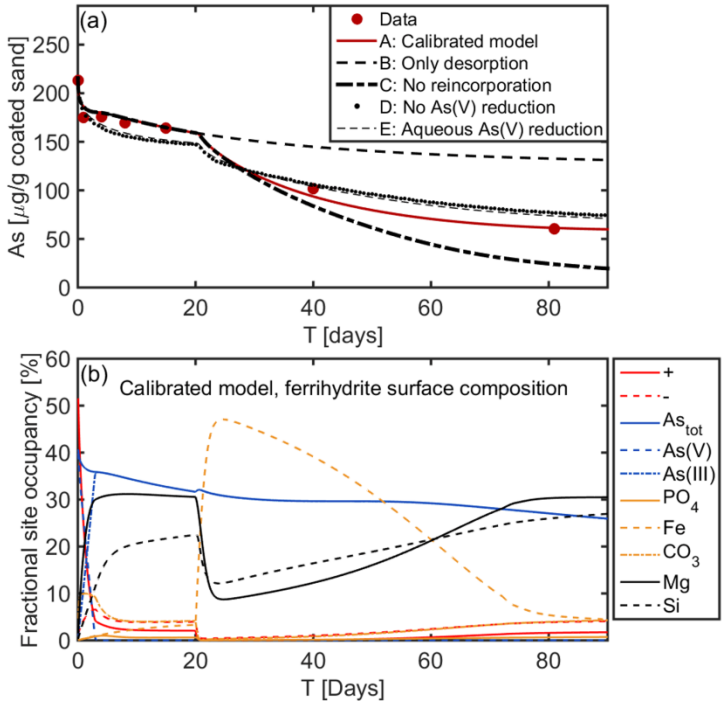

Figure 3. (a) Temporal change in total solid-associated arsenic concentration predicted for well 4-5 when considering different mechanisms of As sequestration and change of speciation. (b) Simulated temporal change in composition of the weak sites (i.e., Hfo_w) of ferrihydrite in well 4-5 obtained with the calibrated model.

When discarding the iron mineral transformation and only considering As desorption (i.e. Scenario A), the model captures well the first experimental observations but simulates significantly higher As surface concentration after 25 days when ferrihydrite dissolution becomes relevant. This scenario yields a concentration of 133.2 µg As/g coated sand at the end of the experiments that is more than twice the observed value 60.4 µg As/g coated sand (Figure 3a). This difference shows that the As release from ferrihydrite surface is primarily determined

by the decrease in available sorption sites induced by the disintegration of ferrihydrite whereas sorption competition is of lower importance when reductive dissolution takes place in agreement with the observations of Root et al. *(9)* on artificially deposited ferrihydrite-rich sediments of the North Haiwee Reservoir (Olancha, CA, USA). Conversely, the model scenario that does not include uptake of arsenic into newly formed minerals predicts higher release of arsenic and, thus, lower As concentration at the end of the experiments (i.e., 24.2 µg As/g coated sand at 80 days). These simulation results underpin the importance of As sequestration into secondary minerals for the observed behavior at the field site.

Direct microbially-mediated reduction of aqueous and/or adsorbed As(V) has been extensively observed during transition from aerobic to anaerobic conditions *(30-31)*. However, the sequential order in which the biotic reduction of Fe(III) oxide minerals and As(V) occur has been debated *(14, 30, 81-83)*. Furthermore, it remains unclear whether bacteria can directly transform the As(V) into As(III) on the surface or initially requires the desorption of As(V). Here, the speciation change of surface-associated As(V) led to the best agreement with the field dataset. In particular, this mechanism is predicted to limit the release of As from ferrihydrite as a stronger initial As release that is predicted when reduction of surface As(V) is not considered (Scenarios D and E in Figure 3a). When analyzing the simulated temporal change in surface composition (Figure 3b), the adsorbed As(V) becomes As(III) at early times of the in-situ experiments preceding the reductive dissolution of ferrihydrite (e.g., 7 days in well 4-5).

The solid-associated As at the end of the experiment days was predicted as As(III) whereas the speciation determined by K-edge XANES measurements indicated As(V) as the dominant species (Table SI3). This discrepancy may result from the oxidation of As(III) via interaction

354 and/or sequestration into the formed crystalline iron phases as observed by Amstaetter et al. *(76)*.
355 Indeed, the model indicates that the main part of the solid-associated As (i.e., 80% and 62% in
356 wells 5-2 and 4-5, respectively) is sequestered by the secondary iron oxides at the end of the in-
357 situ experiments.

358 At the beginning of the in-situ experiment, a significant part of the As(V) rapidly desorbs (i.e.,
359 49 to 35 % surface sites occupancy; Figure 3b). A sensitivity analysis assessing the effect of the
360 aqueous species on the surface composition of ferrihydrite indicates that this desorption is
361 induced by the rapid drop in surface charge primarily due to the re-equilibration of the
362 ferrihydrite surface with the groundwater and, to a lower extent, to the competitive sorption
363 effects of dissolved bicarbonate and silica (see Supplementary Information, Figure SI4). Due to
364 the local hydrochemical conditions and the high As(III) concentrations in the groundwater, none
365 of the aqueous species seems able to substantially compete for As(III) sorption sites as shown by
366 the steady As(III) fractional site occupancy (Figure 3b) leading to a plateau regime in the As
367 surface concentration until As(III) mobilization is triggered by the disintegration of ferrihydrite
368 (Figure 3a). In particular, the As(III) surface site occupancy remains steady at the onset of
369 microbial dissolution of ferrihydrite (i.e., 20 days) characterized by an abrupt change in surface
370 composition due to the strong adsorption of Fe(II) concomitant to a sharp desorption in Mg and
371 Si. Similar behavior of As adsorbed onto ferrihydrite is predicted in the other wells even though
372 the sequestration of As into secondary mineral phases spatially differ (Supporting Information,
373 Figure SI1 and Table SI6).

374 ***Reductive transformation of ferrihydrite.*** The reductive transformation of ferrihydrite
375 significantly controls the As release through the dissolution of the solid phase. This leads to a

reduction of sorption sites and to the formation of new mineral phases that can potentially sequester arsenic. The model allowed us to assess the relative contribution of the reductive dissolution, Fe(II)-catalyzed transformation, and precipitation of Fe(II)-mineral phases on the change in the total Fe content and in the composition of the mineral assemblage. Figure 4 displays the simulation results obtained when considering individually these iron mineral transformation mechanisms through the definition of four different modeling scenarios:

- Scenario 1: calibrated model (same as Scenario A above);
- Scenario 2: only reductive dissolution of ferrihydrite with no further Fe(II) reactions (i.e., no Ostwald ripening and no Fe(II) precipitation with carbonate and sulfide);
- Scenario 3: as Scenario 2 but including Fe(II) precipitation with carbonate and sulfide;
- Scenario 4: Fe(II) allowed to react with ferrihydrite through Ostwald ripening but without reductive dissolution.

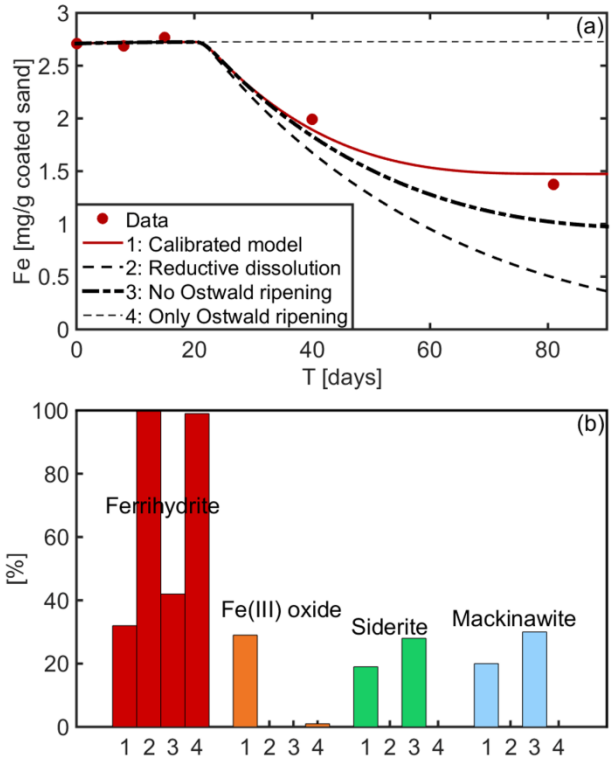

388

389 Figure 4. (a) Temporal change in total Fe content assessed through the different model scenarios;
390 (b) composition of the mineral assemblage at 80 days predicted for well 4-5 using the model and
391 considering the contributions of the different transformation mechanisms studied in Scenario 1-4.

392 Figure 4a shows that the observed pattern of Fe content measured in well 4-5 is captured well by
393 the calibrated model (Scenario 1). When only defining the reductive dissolution of ferrihydrite
394 (Scenario 2) the Fe-content is significantly underestimated (e.g., 0.49 mg Fe/g coated sand
395 compared to the experimental observation of 1.37 mg Fe/g coated sand at 80 days). The
396 formation of ferrous iron minerals limits the decrease in solid-associated Fe and improves the
397 agreement with the field data as illustrated by Scenario 3 (e.g., 1.01 mg Fe/g coated sand at 80
398 days). However, this scenario does not include Ostwald ripening and results in a slight
399 underestimation of the Fe content. Finally, Scenario 4 that only considers the effect of Ostwald
400 ripening does not capture the observed behavior. This scenario predicts a constant Fe content,

401 and only minimal conversion of ferrihydrite into Fe(III) oxide compared to Scenario 1. These
402 results suggest that, under the investigated field conditions, the Fe(II) groundwater
403 concentrations are not sufficient to promote significant recrystallization of ferrihydrite and that
404 the reductive dissolution of ferrihydrite is a prerequisite to generate the local Fe(II)
405 concentrations necessary to substantially convert ferrihydrite into Fe crystalline phases. In
406 particular, the comparison between Scenario 1 and Scenario 3 shows that Ostwald ripening
407 improves the agreement with the experimental data, through the preservation of solid-associated
408 Fe, when it is considered together with the reductive dissolution of ferrihydrite and the formation
409 of Fe(II) secondary minerals.

410 ***Fe(II)-induced mineralization pathways.*** The type of secondary minerals, as well as the extent
411 and the kinetics of the conversion of ferrihydrite into more crystalline Fe(III) oxides, are
412 primarily controlled by the supply rate and the magnitude of the aqueous Fe(II) concentration *(21,*
413 *84)*. However, significant differences in the crystallization of ferrihydrite can be observed
414 between the wells despite similar surface and aqueous Fe(II) concentrations simulated upon
415 ferrihydrite dissolution (Figure SI3). This suggests that other mechanisms influence the Fe(II)-
416 induced transformation of ferrihydrite and ultimately the As mobility. Adsorbed trace elements
417 and/or the presence of major ions are known to determine the choice of the Fe(II)-induced
418 mineralization pathway from ferrihydrite *(69, 85)*. In particular, the lower crystallization of
419 ferrihydrite predicted in well 2-4 (Figure 2) might be ascribed to the relatively higher chloride,
420 sulfate and bicarbonate concentrations in that well directly considered in the kinetic rate
421 expression controlling the Ostwald ripening reaction (Equation 2, Table SI2), which is in
422 agreement with previous studies *(69)*. Furthermore, the presence of magnetite that forms through
423 topotactic transformation during Fe(II)-induced crystallization of ferrihydrite was not observed

during the in-situ experiments. Magnetite is typically observed in presence of high ferrous iron concentrations that impede the release of Fe(II) from the mineral and result in a mix Fe(II)-Fe(III) solid *(23-24, 65, 21, 66, 69)*. Despite relatively low dissolved Fe(II) concentration simulated by the model (always less than 1 mM, Figure SI3), the ratio between ferrous iron and ferrihydrite concentrations at which formation of magnetite is typically observed (i.e., 1 mmol Fe(II)/g Hfo *(39)*) was exceeded upon reductive dissolution of ferrihydrite (i.e., [2 - 10] mmol Fe(II)/g Hfo). However, magnetite was not observed during the in-situ experiments. This result can be explained by the relatively low groundwater concentration of Fe(II) that was maintained during the initial phase preceding the onset of ferrihydrite reduction. Over this initial period, accumulation of small amounts of lepidocrocite and/or goethite favored by the action of Fe(II) on ferrihydrite could have led to surface site passivation preventing the formation of magnetite despite the high concentration of Fe(II) occurring upon ferrihydrite reductive dissolution. A similar effect has been observed in controlled laboratory experiments *(64)*.

Implications. The reductive dissolution of poorly crystalline iron oxides has been recognized as one of the predominant pathways leading to As contamination of groundwater *(7, 20)*. However, the complex interplay of geochemical processes in natural groundwater systems hampers a detailed description of the mechanisms controlling the fate and evolution of mineral phases and As release from the sole analysis of water chemistry and mineral characterization data. This study has highlighted the importance of multiple mechanisms (i.e., surface complexation, reductive dissolution, formation of secondary iron minerals and arsenic sequestration into the newly formed minerals), occurring at different time scales and with significant spatial variability, when groundwater contacts ferrihydrite and triggers the release of arsenic. The model-based interpretation of the in-situ experiments was instrumental to disentangle the roles of the different

447 geochemical processes on the evolution of the mineral assemblage and arsenic in the flow-
448 through system. While part of the arsenic rapidly desorbed from ferrihydrite, most of the
449 mobilization of solid-associated arsenic was controlled by the reductive dissolution of the
450 primary mineral and sequestration (i.e., sorption and reincorporation) into secondary iron oxides
451 in agreement with previous laboratory studies *(30)*. Formation of these more crystalline phases
452 was found to be induced by the Fe(II) generated from the disintegration of ferrihydrite triggering
453 further mineral crystallization. The model highlights important implications of different
454 geochemical mechanisms on the evolution of solid-associated iron and, thus, on the release of
455 arsenic. The kinetics of the transformation of ferrihydrite was particularly influenced by the
456 dissolved groundwater species (e.g., charged solutes) through chemical and electrostatic
457 interactions, and by mineral assemblage composition and transformation. The absence of
458 magnetite formation during the in-situ experiment, despite the high level of generated Fe(II),
459 contrasts with previous laboratory studies which extensively reported magnetite formation upon
460 reductive dissolution of ferrihydrite. This calls for further investigation on the mechanisms
461 controlling the mineralization pathway during Fe(II)-catalyzed transformation of ferrihydrite.
462 The outcomes of this modeling study emphasize the importance of detailed experimental
463 observations able to capture the temporal dynamics and the spatial variability of geochemical
464 controls on arsenic mobilization. The determination of solid-associated arsenic and iron
465 concentrations, together with the microscopic and spectroscopic characterization of primary and
466 secondary minerals and the chemistry of the groundwater, contributed to underpin the model-
467 based interpretation.

468 The performed model-based analysis was carried out using a one-dimensional flow-through
469 approach at specific spatial locations where experimental observations were available. The

470 understanding gained on the temporal dynamics and kinetic parameters for the different
471 geochemical processes could be exported and tested in multidimensional flow-through domains,
472 which have additional degrees of freedom whose effects cannot be easily extrapolated from 1-D
473 setups *(86-87)*. The integration of the knowledge on arsenic release and iron transformation in
474 multidimensional reactive transport models of groundwater flow systems will allow the joint
475 consideration of the geochemical complexity, highlighted in this investigation, with the physical
476 and chemical heterogeneity of groundwater flow system *(88-91)*. This will contribute to improve
477 our capability to describe and predict the release, transport, and fate of arsenic in complex,
478 heterogeneous aquifer systems. Such approach based on mechanistic description of physical and
479 biogeochemical processes also represents a promising design tool for remediation strategies
480 based on amendments injection and enhanced reactive mineral transformation.

481
482 **Associated content**

483 ***Supporting Information***

484 Field data: wells technical information, measured groundwater aqueous composition used as
485 input parameters in the reactive transport model, measured time series of total Fe and As, the
486 mineral composition and solid-associated arsenic speciation measured at 80 days. Tables
487 summarizing literature and optimized values of the affinity constants used in the surface
488 complexation models as well as the optimized model parameters. Model results showing the
489 change in surface composition and aqueous composition simulated in other wells. Results of a
490 sensitivity analysis performed to assess the effects of hydrochemical composition on the surface
491 composition of ferrihydrite.

Acknowledgments

This work was funded by the Sino-Danish Center for Education and Research (SDC) with a PhD scholarship granted to L.S. M.R. also acknowledges the support of the Villum Block Fellowship (Villum Fonden, Denmark). G.H. and D.Z. are grateful for the support of the National Natural Science Foundation of China (grant Nos. 41825017 and 41672225) and the Fundamental Research Funds for the Central Universities (grant No. 2652017165).

References

(1) Smedley, P. L.; Kinniburgh, D. G. A review of the source, behaviour and distribution of arsenic in natural waters. *Appl. Geochem.* **2002**, 17(5), 517-568; DOI: 10.1016/S0883-2927(02)00018-5.

(2) Appelo, C.; Postma, D. *Geochemistry, groundwater and pollution*, 2nd, ed.; London: CRC Press, 2005.

(3) Bretzler, A.; Stolze, L.; Nikiema, J.; Lalanne, F.; Ghadiri, E.; Brennwald, M. S.; Rolle, M.; Schirmer, M. Hydrogeochemical and multi-tracer investigations of arsenic-affected aquifers in semi-arid West Africa. *Geosci. Front.* **2018**, In Press, DOI: 10.1016/j.gsf.2018.06.004.

(4) Fendorf, S.; Michael, H. A.; van Geen, A. Spatial and temporal variations of groundwater arsenic in South and Southeast Asia. *Science* **2010**, 328(5982), 1123-1127; DOI: 10.1126/science.1172974.

(5) Berg, M.;Tran, H. C.; Nguyen, T. C.; Pham, H. V.; Schertenleib, R.; Giger, W. Arsenic contamination of groundwater and drinking water in Vietnam: a human health threat. *Environ. Sci. Technol.* **2001**, 35(13), 2621-2626; DOI: 10.1021/es010027y.

(6) Harvey, C. F.; Swartz, C. H.; Badruzzaman, A. B. M.; Keon-Blute, N.; Yu, W.; Ali, M. A.; Jay, J.; Beckie, R.; Niedan, V.; Brabander, D.; Oates, P. M.; Ashfaque, K. N.; Islam, S.; Hemond, H. F.; Ahmed, M. F. Arsenic mobility and groundwater extraction in Bangladesh. *Science* **2002**, 298(5598), 1602-1606; DOI: 10.1126/science.1076978.

(7) Meharg, A. A.; Scrimgeour, C.; Hossain, S. A.; Fuller, K.; Cruickshank, K.; Williams, P. N.; Kinniburgh, D. G. Codeposition of organic carbon and arsenic in Bengal delta aquifers. *Environ. Sci. Technol.* **2006**, 40, 4928-4935; DOI: 10.1021/es060722b.

(8) Mladenov, N.; Zheng, Y.; Miller, M. P.; Nemergut, D. R.; Legg, T.; Simone, B.; Hageman, C.; Rahman, M. M.; Ahmed, K. M.; McKnight, D. M. Dissolved organic matter sources and consequences for iron and arsenic mobilization in Bengladesh aquifers. *Environ. Sci. Technol.* **2010**, 44(1), 123-128; DOI: 10.1021/es901472g.

(9) Root, R. A.; Dixit, S.; Campbell, K. M.; Jew, A. D.; Hering, J. G.; O'Day, P. A. Arsenic sequestration by sorption processes in high-iron sediments. *Geochim. Cosmochim. Acta* **2007**, 71(23), 5782-5803; DOI: 10.1016/j.gca.2007.04.038.

(10) Jessen, S.; Postma, D.; Larsen, F.; Nhan, P. Q.; Hoa, L. Q.; Trang, P. T. K.; Long, T. V.; Viet, P. H.; Jakobsen, R. Surface complexation modeling of groundwater arsenic

mobility: Results of a forced gradient experiment in a Red River flood plain aquifer, Vietnam. *Geochim. Cosmochim. Acta* **2012**, 98, 186-201; DOI: 10.1016/j.gca.2012.07.014.

(11) Wang, L.; Giammar, D. E. Effects of pH, dossolved oxygen, and aqueous ferrous iron on the adsorption of arsenic to lepidocrocite. *J. Colloid Interface Sci.* **2015**, 448, 331-338; DOI: 10.1016/j.jcis.2015.02.047.

(12) Postma, D.; Trang, P.T.K.; Sø, H.U.; Hoan, H.V.; Lan, V.M.; Thai, N.T.; Larsen, F.; Viet, P.H.; Jakobsen, R. A model for the evolution in water chemistry of an arsenic contaminated aquifer over the last 6000 years, Red River floodplain, Vietnam. *Geochim. Cosmochim. Acta.* **2016**, 195, 277-292; DOI: .1016/j.gca.2016.09.014.

(13) Sø, H. U.; Postma, D.; Hoang, V. H.; Mai, L. V.; Kim, T. P. T.; Hung, V. P.; Jakobsen, R. Arsenite adsorption controlled by the iron oxide content of Holocene Red River aquifer sediment. *Geochim. Cosmochim. Acta.* **2018**, 239, 61-73; DOI: 10.1016/j.gca.2018.07.026.

(14) Campbell, K. M.; Malasarn, D.; Saltikov, C. W.; Newman, D. K.; Hering, J. G. Simultaneous microbial reduction of iron(III) and arsenic(V) in suspensions of hydrous ferric oxide. *Environ. Sci. Technol.* **2006**, 40(19), 5950-5955; DOI: 10.1021/es0600476.

(15) Tufano, K. J.; Reyes, C.; Saltikov, C.; Fendorf, S. Reductive processes controlling arsenic retention: revealing the relative importance of iron and arsenic retention. *Environ. Sci. Technol.* **2008**, 42, 8283-8289; DOI: 10.1021/es801059s.

(16) Tufano, K. J.; Fendorf, S. Confounding impacts of iron reduction on arsenic retention. *Environ. Sci. Technol.* **2008**, 42(13), 4777-4783; DOI: 10.1021/es702625e.

(17) Dixit, S.; Hering, J. G. Comparison of Arsenic(V) and Arsenic(III) sorption onto iron oxide minerals: implications for arsenic mobility. *Environ. Sci. Technol.* **2003**, 37(18), 4182-4188; DOI: 10.1021/es030309t.

(18) Akai, J.; Izumi, K.; Fukuhara, H.; Masuda, H.; Nakano, S.; Yoshimura, T.; Ohfuji, H.; Md Anawar, H.; Akai, K. Mineralogical and geomicrobiological investigations on groundwater arsenic enrichment in Bengladesh. *Appl. Geochem.* **2004**, 19(2), 215-230; DOI: 10.1016/j.apgeochem.2003.09.008.

(19) Sun, J.; Mailloux, B. J.; Chillrud, S. N.; van Geen, A.; Thompson, A.; Bostick, B. C. Simultaneously quantifying ferrihydrite and goethite in natural sediments using the method of standard additions with X-ray absorption spectroscopy. *Chem. Geol* **2018a**, 476, 248-259; DOI: 10.1016/j.chemgeo.2017.11.021.

(20) Stuckey, J. W.; Schaefer, M. V.; Benner, S. G.; Fendorf, S. Reactivity and speciation of mineral-associated arsenic in seasonal and permanent wetlands of the Mekong Delta. *Geochim. Cosmochim. Acta* **2015a**, 171, 143-155; DOI: 10.1016/j.gca.2015.09.002.

(21) Zachara, J. M.; Kukkadapu, R. K.; Frederickson, J. K.; Gorby, Y. A.; Smith, S. C. Biomineralization of poorly crystalline Fe(III) oxides by dissimilatory metal reducing bacteria (DMRB). *Geomicrobiol. J.* **2002**, 19, 179-207; DOI: 10.1080/01490450252864271.

(22) Weber, K. A.; Achenbach, L. A.; Coates, J. D. Microorganisms pumping iron: anaerobic microbial iron oxidation and reduction. *Nat. Rev. Microbiol.* **2006**, 4, 752-764; DOI: 10.1038/nrmicro1490.

(23) Benner, S; Hansel, C. M.; Wielinga, B. W.; Barber, T. M.; Fendorf, S. Reductive dissolution and biomineralization of iron hydroxide under dynamic flow conditions. *Environ. Sci. Technol.* **2002**, 36(8), 1705-1711; DOI: 10.1021/es0156441.

(24) Pedersen, H. D.; Postma, D.; Jakobsen, R.; Larsen, O. Fast transformation of iron oxyhydroxides by the catalytic action of aqueous Fe(II). *Geochim. Cosmochim. Acta* **2005**, 69(16), 3967-3977; DOI: 10.1016/j.gca.2005.03.016.

(25) Yang, L.; Steefel, C. I.; Marcus, M. A.; Bargar, J. R. Kinetics of Fe(II)-catalyzed transformation of 6-line ferrihydrite under anaerobic conditions. *Environ. Sci. Technol.* **2010**, 44(14), 5469-5475; DOI: 10.1021/es1007565.

(26) Boland, D. D.; Collins, R. N.; Miller, C. J.; Glover, C. J.; Waite, T. D. Effect of solution and solid-phase conditions on the Fe(II)-accelerated transformation of ferrihydrite to lepidocrocite and goethite. *Environ. Sci. Technol.* **2014**, 48(10), 5477-5485, DOI: 10.1021/es4043275.

(27) Kocar, B. D.; Fendorf, S. Thermodynamic constraints on reductive reactions influencing the biogeochemistry of arsenic in soils and sediments. *Environ. Sci. Technol.* **2009**, 43, 4871-4877; DOI: 10.1021/es8035384.

(28) Ford, R. Rates of hydrous ferric oxide crystallization and the influence on coprecipitated arsenate. *Environ. Sci. Technol.* **2002**, 36(11), 2459-2463; DOI: 10.1021/es015768d.

(29) Islam, F. S.; Pederick, R. L.; Gault, A. G.; Adams, L. K.; Polya, D. A.; Charnock, J. M.; Lloyd, J. R. Interactions between the Fe(III)-reducing bacterium Geobacter sulfurreducens and arsenate, and capture of the metalloid by biogenic Fe(II). *Appl. Environ. Microbiol.* **2005**, 71(12), 8642-8648; DOI: 10.1128/AEM.71.12.8642-8648.2005.

(30) Herbel, M. J.; Fendorf, S. Biogeochemical processes controlling the speciation and transport of arsenic within iron coated sands. *Chem. Geol.* **2006**, 228(1-3), 16-32; DOI: 10.1016/j.chemgeo.2005.11.016.

(31) Kocar, B. D.; Herbel, M. J.; Tufano, K. J.; Fendorf, S. Contrasting effects of dissimilatory iron (III) and arsenic (V) reduction on arsenic retention and transport. *Environ. Sci. Technol.* **2006***,* 40(21), 6715-6721; DOI: 10.1021/es061540k.

(32) Pedersen, H. D.; Postma, D.; Jakobsen, R. Release of arsenic associated with the reduction and transformation of iron oxides. *Geochim. Cosmochim. Acta* **2006**, 70, 4116-4129; DOI: 10.1016/j.gca.2006.06.1370.

(33) Neidhardt, H.; Berner, Z. A.; Freikowski, D.; Biswas, A.; Majumder, S.; Winter, J.; Gallert, C.; Chatterjee, D.; Norra, S. Organic carbon induced mobilization of iron and manganese in a West Bengal aquifer and the muted response of groundwater arsenic concentrations. *Chem. Geol.* **2014**, 367, 51-62; DOI: 10.1016/j.chemgeo.2013.12.021.

(34) Rawson, J.; Siade, A.; Sun, J.; Neidhardt, H.; Berg, M.; Prommer, H. Quantifying reactive transport processes governing arsenic mobility after injection of reactive organic carbon into a Bengal Delta aquifer. *Environ. Sci. Technol.* **2017**, 51(15), 8471-8480; DOI: 10.1021/acs.est.7b02097.

(35) Nielsen, S.; Kjeldsen, P.; Bruun Hansen, H.; Jakobsen, R. Transformation of natural ferrihydrite aged in situ in As, Cr and Cu contaminated soil studied by reduction kinetics. *Appl. Geochem.* **2014**, 51, 293-302; DOI: 10.1016/j.apgeochem.2014.10.014.

(36) Stuckey, J. W.; Schaefer, M. V.; Kocar, B. D.; Benner, S. G.; Fendorf, S. Arsenic release metabolically limited to permanently water-saturated soil in Mekong Delta. *Nat. Geosci.* **2015b**, 9, 70-78; DOI: 10.1038/ngeo2589.

(37) Zhang, Di; Guo, H.; Xiu, W.; Ni, P.; Zheng, H.; Wei, C. In-situ mobilization and transformation of iron oxides-adsorbed arsenate in natural groundwater. *J. Hazard. Mater.* **2017**, 321, 228-237; DOI: 10.1016/j.jhazmat.2016.09.021.

(38) Neidhardt, H.; Winkel, L. H. E.; Kaegi, R.; Stengel, C.; Trang, P. T. K.; Lan, V. M.; Viet, P. H.; Berg, M. Insights into arsenic retention dynamics of Pleistocene aquifer sediments by in situ sorption experiments. *Water Res.* **2018**, 129, 123-132; DOI: 10.1016/j.watres.2017.11.018.

(39) Tufano, K. J.; Benner, S. G.; Mayer, K. U.; Marcus, M. A.; Nico, P. S.; Fendorf, S. Aggregate-scale heterogeneity in iron (hydr)oxide reductive transformations. *Vadose Zone J.* **2009**, 8(4), 1004-1012; DOI: 10.2136/vzj2008.0090.

(40) Sharma, P.; Rolle, M.; Kocar, B.; Fendorf, S.; Kappler, A. Influence of natural organic matter on As transport and retention. *Environ. Sci. Technol.* **2011**, 45, 546-553; DOI: 10.1021/es1026008

(41) Rawson, J.; Prommer, H.; Siade, A.; Carr, J.; Berg, M.; Davis, J. A.; Fendorf, S. Numerical modeling of arsenic mobility during reductive iron-mineral transformations. *Environ. Sci. Technol.* **2016**, 50(5), 2459–2467; DOI: 10.1021/acs.est.5b05956.

(42) Sun, J.; Prommer, H.; Siade, A.J.; Chillrud, S. N.; Mailloux, B. J.; Bostick, B. C. Model-based analysis of arsenic immobilization via iron mineral transformation under advective flows. *Environ. Sci. Technol.* **2018b**, 52(16), 9243-9253; DOI: 10.1021/acs.est.8b01762.

(43) Postma, D.; Larsen, F.; Hue, N.T.M.; Duc, M.T.; Viet, P.H.; Nhan, P.Q.; Jessen, S. Arsenic in groundwater of the Red River floodplain, Vietnam: Controlling geochemical processes and reactive transport modeling. *Geochim. Cosmochim. Acta.* **2007**, 71, 5054-5071; DOI: 10.1016/j.gca.2007.08.020.

(44) Kocar, B.D.; Polizotto, M.L.; Benner, S.G.; Ying, S.C.; Ung, M.; Ouch, K.; Samreth, S.; Suy, B.; Phan, K.; Sampson, M.; Fendorf, S. Integrated biogeochemical and hydrologic processes driving arsenic release from shallow sediments to groundwaters of the Mekong delta. *Appl. Geochem.* **2008**, 23, 3059-3071; DOI: 10.1016/j.apgeochem.2008.06.026

(45) Stolze, L.; Zhang, D.; Guo, H.; Rolle, M. Surface complexation modeling of arsenic mobilization from goethite: Interpretation of an in-situ experiment. *Geochim. Cosmochim. Acta* **2019**, 248, 274-288; DOI: 10.1016/j.gca.2019.01.008.

(46) Schwertmann, U.; Cornell, R.M. *Iron oxides in the laboratory - Preparation and characterization*; Wiley-VCH: Weinheim, 2000.

(47) Link, D.D.; Walter, P.J.; Kingston, H.M. Development and validation of the new EPA microwave-assisted leach method 3051A. *Environ. Sci. Technol.* **1998**, 32(22), 3628-3632; DOI: 10.1021/es980559n

(48) Parkhurst, D. L.; Appelo, C. A. J., 2013. Description of input and examples for PHREEQC version 3 - A computer program for speciation, batch-reaction, one-dimensional transport, and inverse geochemical calculations. In: *U.S. Geological Survey Techniques amd Methods,* book 6, chap. A43, p. 497.

(49) Haberer, C.; Muniruzzaman, M.; Grathwohl, P; Rolle, M. Diffuse-dispersive and reactive fronts in porous media. Vadose Zone J. **2015**, 14(5), 1-14, DOI: 10.2136/vzj2014.07.0091.

(50) Rolle, M.; Sprocati, R.; Masi, M.; Jin, B.; Muniruzzaman, M. Nernst-Planck based description of transport, coulombic interactions and geochemical reactions in porous media: modeling approach and benchmark experiments. *Water Resour. Res.* **2018**, 54(4), 3176-3195; DOI: 10.1002/2017WR022344.

(51) Charlton, S. R.; Parkhurst, D. L. Modules based on the geochemical model PHREEQC for use in scripting and programming languages. *Comput. Geosci.* 2011, 37, 1653-1663.

(52) Muniruzzaman, M.; Rolle, M. Modeling multicomponent ionic transport in groundwater with IPhreeqc coupling: Electrostatic interactions and geochemical reactions in homogeneous and heterogeneous domains. *Adv. Water Resour.* **2016**, 98, 1-15; DOI: 10.1016/j.advwatres.2016.10.013.

(53) Schecher, W. D.; McAvoy, D. C. MINEQL+, V. 4.5, Users Manual, Hallowell, ME, 1998.

(54) Langmuir, D. The Gibbs free energies of substances in the system Fe-O_2-H_2O-CO_2 at 25C. In: *Geological Survey research*; USGS Prof. pap. 650-B; U.S. Gov. Print. Office, Washington, DC. 1969; pp B180-B183.

(55) Nordstrom, D. K.; Plummer, L. N.; Langmuir, D.; Busenberg, E.; May, H. M.; Jones, B. F.; Parkhurst, D. L. Revised chemical equilibrium data for major water-mineral reactions and their limitations. In: *Chemical Modeling of Aqueous Systems II*, Bassett, R.L., Melchior, D., Eds.; American Chemical Society Symposium Series 416, 1990, pp 398-413.

(56) Burton, E. D.; Johnston, S. G.; Bush, R. T. Microbial sulfidogenesis in ferrihydrite-rich environments : Effects on iron mineralogy and arsenic mobility. *Geochim. Cosmochim. Acta* **2011**, 75(11), 3072-3087; DOI: 10.1016/j.gca.2011.03.001.

(57) Van Capellen, P; Gaillard, J.-F. Biogeochemical dynamics in aquatic sediments. In: *Reactive transport in porous media.* Lichtner P. C., Steefel C. I., Oelkers E. H. Eds.; The Mineralogical Society of America, Washington DC 1996; 335-376.

(58) Pallud, C.; Kausch, M.; Fendorf, S.; Meile, C. Spatial patterns and modeling of reductive ferrihydrite transformation observed in artifical soil aggregates. *Environ. Sci. Technol.* **2010**, 44(1), 74-79; DOI: 10.1021/es901736t.

(59) Roden, E. E. Fe(III) oxide reactivity toward biological versus chemical reduction. *Environ. Sci. Technol.* **2003**, 37, 1319-1324; DOI: 10.1021/es026038o.

(60) Roden, E. E.; Urrutia, M. M. Ferrous iron removal promotes microbial reduction of crystalline iron(III) oxides. *Environ. Sci. Technol.* **1999**, 33, 1847-1853; DOI: 10.1021/es9809859.

(61) Borch, T.; Masue, Y.; Kukkadapu, R. K.; Fendorf, S. Phosphate imposed limitations on biological reduction and alteration of ferrihydrite. *Environ. Sci. Technol.* **2007**, 41(1), 166-172; DOI: 10.1021/es060695p.

(62) Jia, Y.; Guo, H.; Jiang, Y.; Wu, Y. ; Zhou, Y. Hydrogeochemical zonation and its implication for arsenic mobilization in deep groundwaters near alluvial fans in the Hetao Basin, Inner Mongolia. *J. Hydrol.* **2014**, 518, 410-420; DOI: 10.1016/j.jhydrol.2014.02.004.

(63) Cornell, R.; Schwertmann, U. *The Iron oxides: Structure, Properties, Reactions, Occurrence and Uses*; Wiley-VCH: Weinheim, 2003.

(64) Hansel, C. M.; Benner, S. G.; Neiss, J.; Dohnalkova, A.; Kukkadapu, R. K.; Fendorf, S. Secondary mineralization pathways induced by dissimilatory iron reduction of ferrihydrite under advective flow. *Geochim. Cosmochim. Acta* **2003**, 67(16), 2977-2992; DOI: 10.1016/S0016-7037(03)00276-X.

(65) Tronc, E.; Belleville, P.; Jolivet, J.-P.; Livage, J. Transformation of ferric hydroxide into spinel by iron(II) adsorption. *Langmuir* **1992**, 8(1), 313-319; DOI: 10.1021/la00037a057.

(66) Jeon, B.; Dempsey, B. A.; Burgos, W. D. Kinetics and mechanisms for reactions of Fe(II) with iron(III) oxides. *Environ. Sci. Technol.* **2003**, 37(15), 3309-3315; DOI: 10.1021/es025900p.

(67) Williams, A. G. B.; Scherer, M. M. Spectroscopic evidence for Fe(II)-Fe (III) electron transfer at the iron oxide-water interface. *Environ. Sci Technol.* **2004**, 38(18), 4782-4790; DOI: 10.1021/es049373g.

(68) Boland, D. D.; Collins, R. N.; Glover, C. J.; Waite, T. D. An in situ quick-EXAFS and redox potential study of the Fe(II)-catalysed transformation of ferrihydrite. *Colloids Surf. A* **2013**, 435, 2-8; DOI: 10.1016/j.colsurfa.2013.02.009.

(69) Hansel, C. M., Benner, S. G.; Fendorf, S. Competing Fe(II)-induced mineralization pathways of ferrihydrite. *Environ. Sci. Technol.* **2005**, 39(18), 7147-7153; DOI: 10.1021/es050666z.

(70) Dzombak, D. A.; Morel, F. M. *Surface Complexation Modeling: Hydrous Ferric Oxide*; John Wiley & Sons: New York, 1990.

(71) Mathur, S.; Dzombak, D. A. Surface complexation modeling: Goethite. In: *Surface Complexation Modeling 1st Edition,* Lützenkirchen J., Ed.; London: Elsevier Ltd. 2006, pp 443-467.

730 (72) Pierce, M. L.; Moore, C. B. Adsorption of arsenite and arsenate on amorphous iron
731 hydroxide. *Water Res.* **1982**, 16(7), 1247-1253; DOI: 10.1016/0043-1354(82)90143-9.

732 (73) Gustafsson, J.; Bhattacharya, P. Geochemical modelling of arsenic adsorption to oxide
733 surfaces. In *Arsenic in Soil and Groundwater Environment*; Bhattacharya, P.,
734 Mukherjee, A. B., Bundschuh, J., Zevenhoven, R., Loeppert, R. H., Eds.; Elsevier B.V.
735 2007; pp 159-206.

736 (74) Swedlund, P. J.; Webster, J. G. Adsorption and polymerisation of silicic acid on
737 ferrihydrite, and its effect on arsenic adsorption. *Water Res.* **1999**, 33(16), 3413-3422;
738 DOI: 10.1016/S0043-1354(99)00055-X.

739 (75) Appelo, C. A. J.; Van Der Weiden, M. J. J.; Tournassat, C.; Charlet, L. Surface
740 complexation of ferrous iron and carbonate on ferrihydrite and the mobilization of
741 arsenic. *Environ. Sci. Technol.* **2002**, 36(14), 3096-3103; DOI: 10.1021/es010130n.

742 (76) Amstaetter, K.; Borch, T.; Larese-Casanova, P.; Kappler, A. Redox transformation of
743 arsenic by Fe(II)-activated goethite (r-FeOOH). *Environ. Sci. Technol.* **2010**, 44(1),
744 102-108; DOI: 10.1021/es901274s.

745 (77) Kirk, M. F.; Roden, E. E.; Crossey, L. J.; Brealey, A. J.; Spilde, M. N. Experimental
746 analysis of arsenic precipitation during microbial sulfate and iron reduction in model
747 aquifer sediment reactors. *Geochim. Cosmochim. Acta* **2010**, 74(9), 2538-2555; DOI:
748 10.1016/j.gca.2010.02.002.

749 (78) Kocar, B. D.; Borch, T.; Fendorf, S. Arsenic repartitioning during biogenic sulfidization
750 and transformation of ferrihydrite. *Geochim. Cosmochim. Acta* **2010**, 74(3), 980-994;
751 DOI: 10.1016/j.gca.2009.10.023.

752 (79) Rathi, B.; Neidhardt, H.; Berg, M.; Siade, A.; Prommer, H. Processes governing arsenic
753 retardation on Pleistocence sediments: Adsorption experiments and model-based
754 analysis. *Water Resour. Res.* **2017**, 53, 4344-4360; DOI: 10.1002/2017WR020551.

755 (80) Schittich, A.R.; Wünsch, U.J.; Kulkarni, H.V.; Battistel, M.; Bregnhøj, H.; Stedmon,
756 C.A.; McKnight, U.S. Investigating fluorescent organic-matter composition as a key
757 predictor for arsenic mobility in groundwater aquifers. *Environ. Sci. Technol.* **2018**,
758 52(22), 13027-13036; DOI: 10.1021/acs.est.8b04070.

759 (81) Zobrist, J.; Dowdle, P. R.; Davis, J. A.; Oremland, R. S. Mobilization of arsenite by
760 dissimilatory reduction of adsorbed arsenate. *Environ. Sci. Technol.* **2000**, 34, 4747-
761 4753; DOI: 10.1021/es001068h.

(82) Islam, F. S.; Gault, A. G.; Boothman, C.; Polya, D. A.; Charnock, J. M.; Chatterjee, D.; Lloyd, J. R. Role of metal-reducing bacteria in arsenic release from Bengal delta sediments. *Nature* **2004**, 430, 68-71; DOI: 10.1038/nature02638.

(83) Burnol, A.; Garrido, F.; Baranger, P.; Joulian, C.; Dictor, M.-C.; Bodenan, F.; Morin, G.; Charlet, L. Decoupling of arsenic and iron release from ferrihydrite suspension under reducing conditions: a biogeochemical model. *Geochem. Trans.* **2007**, 8(12), 1-18; DOI: 10.1186/1467-4866-8-12.

(84) Hansel, C. M. Bacterial and Geochemical controls on the reductive dissolution and secondary mineralization of iron (hydr)oxides. Ph.D. Dissertation, Stanford University, Stanford, CA, 2004.

(85) Hansel, C. M.; Learman, D. R.; Lentini, C. J.; Ekstrom, E. B. Effect of adsorbed and substituted Al on Fe(II)-induced mineralization pathways of ferrihydrite. *Geochim. Cosmochim. Acta* **2011**, 75(16), 4653-4666; DOI: 10.1016/j.gca.2011.05.033.

(86) Ye, Y. Chiogna, G.; Cirpka, O. A.; Grathwohl, P. Rolle, M. Experimental investigation of compound-specific dilution of solute plumes in saturated porous media: 2-D vs. 3-D flow-through systems. *J. Contam. Hydrol.* **2015a**, 172, 33-47; DOI: 10.1016/j.jconhyd.2014.11.002.

(87) Ye, Y.; Chiogna, G.; Cirpka, O. A.; Grathwohl, P.; Rolle, M. Enhancement of plume dilution in three-dimensional porous media by flow-focusing in high-permeability inclusions. *Water Resour. Res.* **2015b**, 51, 5582-5602; DOI: 10.1002/2015WR016962.

(88) Li, L.; Salehikhoo, F.; Brantley, S. L.; Heidari, P. Spatial zonation limits magnesite dissolution in porous media. *Geochim. Cosmochim. Acta* **2014**, 126, 555-573; DOI: 10.1016/j.gca.2013.10.051.

(89) Muniruzzaman, M.; Haberer, C. M.; Grathwohl, P.; Rolle, M. Multicomponent ionic dispersion during transport of electrolytes in heterogeneous porous media: Experiments and model-based interpretation. *Geochim. Cosmochim. Acta* **2014**, 141, 656-669; DOI: 10.1016/j.gca.2014.06.020.

(90) Wen, H.; Li, L. An upscaled rate law for mineral dissolution in heterogeneous media: The role of time and length scales. *Geochim. Cosmochim. Acta* **2018**, 235, 1-20; DOI: 10.1016/j.gca.2018.04.024.

(91) Battistel, M.; Muniruzzaman, M.; Onses, F.; Lee, J.; Rolle, M. Reactive fronts in chemically heterogeneous porous media: Experimental and modeling investigation of pyrite oxidation. *Appl. Geochem.* **2019**, 100, 77-89; DOI: 10.1016/j.apgeochem.2018.10.026.